



## Novel kappa-carrageenan– poly (vinyl alcohol) – modified pumice hydrogel composite for the adsorption of cationic dye

Ammar M. Mahmoud<sup>1</sup>, Ali A. Ali<sup>1</sup>, Malek Alshukur<sup>4</sup>, Mohamed E. Sultan<sup>1</sup>,  
Hamida Y. Mostafa<sup>2</sup>, E. A. Eldeeb<sup>3</sup>, Ashraf M. Ashmawy<sup>1</sup>



<sup>1</sup> Chemistry Department, Faculty of Science (Boys), Al-Azhar University, 11884, Nasr City, Cairo, Egypt

<sup>2</sup> Refining Department, Egyptian Petroleum Research Institute (EPRI), 1 Ahmed El- Zomor St., Nasr City, 11727, Cairo, Egypt

<sup>3</sup> Environmental studies, institute of graduate studies and research, Alexandria University, Egypt

<sup>4</sup> Department of Mechanical Engineering of Textile Industries and Technologies, Faculty of Mechanical and Electrical Engineering, Damascus University, Damascus, Syrian Arab Republic

### Abstract

In this work, a new resin that can remove cationic dyes like Methylene Blue dye from aqueous solutions will be introduced. For this, novel kappa-carrageenan/polyvinyl alcohol hydrogel (kC/PVA) composites with modified pumice were made. Using the freezing-thawing procedure, the mixture of polymers and modified pumice was cross-linked, and then K<sup>+</sup> ions were added. Using SEM, FTIR, and XRD methods, the structure of the resultant hydrogel composites was identified. Using a batch adsorption technique, the effects of contact time, changed pumice content, temperature, pH, ion strength, and dye solution salinity on the adsorption of cationic methylene blue dye on the hydrogel composites were examined. The swelling capacity of the resultant hydrogels was found to be lower than that of modified pumice-free hydrogels, falling from 780 to 470 %. The number of salts CaCl<sub>2</sub> and AlCl<sub>3</sub> in the solution dramatically reduced the adsorption capacity from 24.61 to 19 and 17 correspondingly. The greatest adsorption capacity of the hydrogel composites achieved was 185.65 mg g<sup>-1</sup>, and equilibrium dye adsorption data were also found to follow the Langmuir model. Based on the results of this study, synthetic hydrogel composites can be used as inexpensive adsorbents to remove colors from aqueous solutions, such as commercial dye baths.

**Keywords:** cationic dye removal; methylene blue dye; modified composite hydrogel; adsorption; kappa-carrageenan; poly (vinyl alcohol); modified pumice.

Key words; Portland cement ; Radioactive waste; Rice Husk ash; Compressive strength; Leaching.

### 1. Introduction

Water resource pollution is a very quarrelsome issue on a worldwide scale, as it has long-term or even deadly significances for living creatures [1]. Water contamination made by dyes is one of the most regarded of these pollutants since it causes alterations in the natural appearance of water even at extremely low quantities.

Dyeing is used in a variety of industries, including textiles, antioxidants, pulp, paper, paint, plastics, rubber, tannery, printer ink, food, and cosmetics [2-8]. There are several dyes available, with an annual production of around 1.6 million tonnes [9]. The release of dyes into the environment

harms aquatic life ecosystems and has a detrimental influence on human health. The effects may cause aesthetic issues like discoloration and unpleasant odors and aquatic ecosystems may be disturbed because of lower sunlight penetration and oxygen depletion in dirty water. The dangers of dye pollution to human health include the possibility of developing skin problems from coming into contact with contaminated water and digestive issues from drinking contaminated water, which may increase the risk of cancer. [10, 11].

Methylene blue (MB), a water dye pollutant, is used in industrial and household beauty items to colour paper, cotton, silk, wool, and hair, among

\*Corresponding author e-mail: [ashraf\\_ashmawy2002@azhar.edu.eg](mailto:ashraf_ashmawy2002@azhar.edu.eg); (Ashraf M. Ashmawy).

Receive Date: 21 November 2022, Revise Date: 24 January 2023, Accept Date: 13 March 2023,

First Publish Date: 13 March 2023

DOI: 10.21608/ejchem.2023.176082.7210

©2023 National Information and Documentation Center (NIDOC)

other things. As a typical cationic organic dye pollutant, MB dye has been widely investigated for its ability to sorb to a wide range of adsorbents [12, 13]. This dye has been linked to a variety of health issues, including ocular, respiratory, digestive, and mental illnesses [14, 15]. Therefore, the removal of this type of dye is of paramount from health perspective as well as environmental perspective [16].

Numerous techniques have been used to study the exclusion of MB dye from industrial waste, such as enzymatic processes, photo-degradation reactions, electrochemical removal, chemical coagulation, membrane separation, and other physical adsorption techniques [17].

One of the methods of removing cationic dyes like methylene blue is the use of hydrogels and hydrogel composites [18].

Hydrogels are cross-linked hydrophilic polymeric polymers that may expand in water without dissolving or losing structural integrity [19]. Hydrogels in aqueous solution can expand or shrink due to binding of different ions and- or to the association, dissociation in their polymer chains [19].

Many materials, such as PVA, kc and pumice, can be used to create composite hydrogels. Several researchers used PVA to create hydrogel composites to PVA /carboxymethyl cellulose(CMC)/ graphene oxide/bentonite and PVA /CMC/ ZSM-5 zeolite [20, 21]. By a physical cross-linking process that happens during freeze-thawing cycles, PVA and its mixes may generate powerful and somewhat stiff hydrogels. PVA crystallites may develop during these cycles, and they can firmly bind the polymer chains in a three-dimensional network [22]. Following many freezing/thawing cycles, several studies discovered hydrogen bonding and crystallite formation between PVA chains. [23-28]. Therefore, PVA and its blends act as robust matrices for the composite hydrogels. Hydrogels of PVA are both transparent and biodegradable while their mechanical properties can be adjusted by the conditions of the cross-linking process [29-31]. PVA-based biopolymer hydrogels are biocompatible, non-carcinogenic, and have reliable physical characteristics [32, 33].

Despite the fact that using three fundamental kinds of carrageenan, only iota and kappa are commonly employed for gel formation [34]. Several articles have described how kC interacts with cations including  $K^+$ ,  $Ca^{2+}$ , and  $Na^+$  to produce ionically cross-linked helical molecules [35-37]. Carrageenan bind to different cations, and the degree of aggregation is highly influenced by the kind and concentration of salt added to the carrageenan solution. On the whole, a Domain model previously examined the mechanism of kC chain crosslinking by  $K^+$  ions. [35], According to this hypothesis, direct intermolecular connection via double helices is restricted to the development of tiny independent domains involving a limited number of chains,

whereas linkage between helices in distinct domains results in greater long-range crosslinking [35].

There are other materials that used of the elimination of cationic ions such as metals, e.g. iron and manganese ions, from water, and modified pumice is one of these materials. Modified pumice is commercialized in the USA as Burgess Iron Removal Media (or simply BIRM). This material is a granulated filter medium containing  $MnO_2$  film on the surface (catalyst) [38] used mainly for iron and manganese removal from water. This media is alumina silicate covered with manganese dioxide, with an operative size of 0.61 mm and a consistency coefficient of 1.72. This material may be used as a substitute media for manganese greensand and is indicated for lower iron concentrations (up to  $6.0\text{ mg l}^{-1}$  for  $Fe^{2+}$  and  $3.0\text{ mg l}^{-1}$  for  $Mn^{2+}$ ) and residential water treatment. When employed as an iron removal medium, BIRM functions as a catalyst, accelerating the interaction between dissolved oxygen (DO) and the iron complexes prevalent in many groundwater sources [39]. It is also suitable for use in gravity and pressure filters. Contact with this filter material causes dissolved iron and manganese to oxidize. Filtration readily removes precipitated Fe and Mn hydroxides (pH of 8 to 9 is necessary for Mn removal) [40].

Due to their potential importance in removing cationic dyes and cations from aqueous solutions, this article describes the method of preparing kc-PVA-modified pumice hydrogel composites for the purpose of removing methylene blue. Methylene blue was used as a model dye to investigate the adsorption behavior of manufactured hydrogels. In summary, the adsorption capacity of such hydrogel composites was studied in different condition of time, temperature or salt additions. Further, the structure of hydrogel composites was studied and the swelling of hydrogel composites was investigated.

## 2. Experimental

### 2.1. Materials

Sigma Aldrich, Germany, provided the polysaccharide and kappa-carrageenan ingredients, while Clack Corporation, USA, provided the modified pumice. This material is manufactured from natural pumice mineral and covered with a very thin layer of manganese dioxide. Denka Chemicals (Japan) provides the poly (vinyl alcohol), PVA, which has a molecular weight (MW) of 89,000-98,000 and a degree of hydrolysis of 99%. Difko Chemical Company (UK) supplied the methylene blue dye (MB), which was utilized without additional purification. The chemical structure of MB is shown in Figure 1, which has a molar mass of  $319.85\text{ g mol}^{-1}$ , color index number is 52015 and maximum peak absorbance  $\lambda_{max}$  is 664 nm [41, 42].

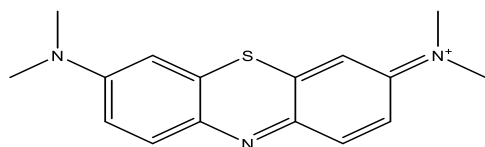


Figure 1. The chemical structure of methylene blue (MB) used in this study.

## 2.2 Preparation of the hydrogel composites

The following is a general process for the synthesis of kC-based hydrogel composites. At 70 °C, 1.0 g of PVA was added to 50 mL of double distilled water. After the PVA was completely dissolved, 1.0 g of kC was additional to the solution and agitated until the kC was completely dissolved. Following this, an appropriate weight of the modified pumice (Birm), in five different cases (0 g, 0.1 g, 0.3 g, 0.6 g, and finally 1 g), was added to the solution and was stirred for 20 min at 70 °C. The resulted solution was then sonicated for 20 min at 80 °C to obtain a homogeneous solution.

The sonicated solutions containing PVA, kC, and modified pumice were first cooled to room temperature before being frozen at -20 °C for 12 hours. The frozen hydrogels were then thawed at room temperature for 5 hours. For each composite hydrogel, the freezing-thawing procedure was done four times. The hydrogels were submerged in 0.5 M of KCl solution for 5 hours after freezing-thawing cycles to create mechanically acceptable hydrogels for subsequent experiments.

For purification, the cross-linked hydrogel composites were submerged in excess distilled water for 12 hours. Finally, the hydrogels were cut into discs with a radius of 0.5 mm and a thickness of 0.4 mm and dried at room temperature until their weights were stable.

Figure 2 depicts a simple approach for generating a new semi-interpenetrating polymer network (semi-IPN) hydrogel composite made of kC and PVA by the integration of modified pumice (Birm). To create composite hydrogels, the mixture was crosslinked in two steps. First, as previously stated, the freezing-thawing process was used to crosslink the PVA component. [43]. Based on this, the PVA molecular chains were entirely connected during the freezing/thawing process via hydrogen bonds. Crystallite production may occur as the PVA chains come into close contact with one other. [23-27]. As a result of the repeated freezing-thawing cycles, physical PVA networks develop a non-degradable three-dimensional structure, resulting in the production of a compact product with great mechanical strength.

Hydrogels were placed into KCl solution for crosslinking of the kC component after four freezing-thawing cycles. Because anionic sulfate groups on kC

backbones can bind electrostatically with  $K^+$  cations [35-37], this leads to crosslink of kC component.

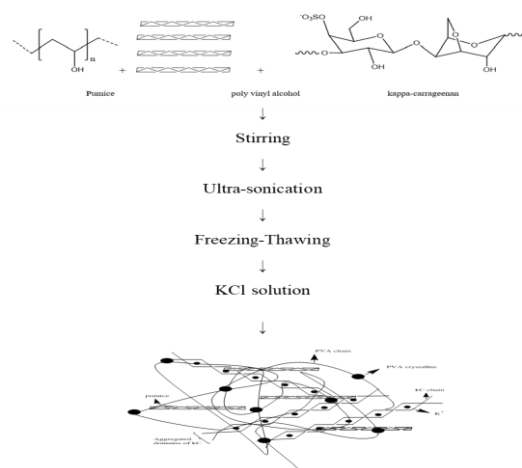


Figure 2 Synthesis of kC-PVA/modified pumice semi-interpenetrating polymer network (IPN) composite hydrogel proposed methodology.

## 2.3 Swelling measurements

The swelling capacity of the hydrogels was changed by using 0.2, 0.4, 0.6, and 1 g of modified pumice for every gramme of PVA and gramme of kappa-carrageenan in order to examine the impact of pumice on the behaviour of the hydrogels when they swell.

Using dried discs, the water absorption capacity of composite hydrogels was assessed. By submerging the Hydrogel composites in 50 mL of distilled water and allowing them to expand at room temperature for 10, 40, 70, 100, 160, 220, and 280 minutes, the equilibrium swelling (ES) capacity of the materials was assessed. After being removed from the aqueous solutions, they were wiped with filter paper to get rid of any surface water, and then weighed. The following equation was used to determine the percentage ES:

$$ES \% = \frac{\text{Weight of swollen hydrogel} - \text{Weight of dried hydrogel}}{\text{Weight of dried hydrogel}} \times 100 \quad (1)$$

## 2.4 Adsorption studies

To achieve MB dye adsorption on the hydrogel composites, 0.05 g of sample was immersed in a dye solution containing 50 mL distilled water and 25 mg  $L^{-1}$  of MB. All adsorption experiments were conducted at ambient temperature (25 °C) in batches and the batches, i.e. the solution and sample, were stirred using a magnetic agitator at a constant speed of 120 revolutions per minute. The solution batches were centrifuged at 3000 revolutions per minute for 10 min before measurements. The content of adsorbed dye was calculated using Equation (2):

$$q_t = \frac{(C_0 - C_t)V}{W} \quad (2)$$

where  $C_0$  is the initial MB concentration ( $mg L^{-1}$ );  $C_t$  is the remaining dye concentration in the solution at

time  $t$ ;  $V$  is the volume of dye solution used (L); and  $W$  (g) is the weight of composite hydrogel.

Adsorption isotherms were carried out by soaking 0.05 g of composites for 24 hours at 25 °C in 50 mL of dye solutions containing 25, 50, 100, 150, and 200 mg L<sup>-1</sup> of MB. Additionally, the equilibrium adsorption capacity of composite hydrogels,  $q_e$ , was determined using equation (2). (mg g<sup>-1</sup>). The equilibrium dye concentration in solution ( $C_e$ ) and equilibrium adsorption capacity ( $q_e$ ), on the other hand, were used to replace  $C_t$  and  $q_t$ . The pH of the original dye solution was adjusted as necessary at room temperature (298K), ambient conditions, by adding 0.1 M HCl to create an acidic solution or 0.1 M NaOH to create a basic solution in order to investigate the impact of pH on adsorption.

Since the presence of salt in dye solutions can affect the adsorption process, we studied the effect of 0.15 M of AlCl<sub>3</sub>, CaCl<sub>2</sub> and NaCl on MB adsorption, pH 8, time 1 hour and the temperature was 298 K (room temperature) at atmospheric conditions.

Because thermodynamic parameters are key components in the design of an adsorption process, it was required to describe the change of thermodynamic parameters in order to determine the feasibility and mechanism of the adsorption process. The thermodynamic parameters studied here including standard Gibbs free energy ( $\Delta G$ , kJ mol<sup>-1</sup>), enthalpy change ( $\Delta H$ , kJ mol<sup>-1</sup>), and entropy change ( $\Delta S$ , J K<sup>-1</sup> mol<sup>-1</sup>). To calculate the values of standard Gibbs free energy ( $\Delta G$ , kJ mol<sup>-1</sup>), enthalpy change ( $\Delta H$ , kJ mol<sup>-1</sup>), and entropy change ( $\Delta S$ , J K<sup>-1</sup> mol<sup>-1</sup>), we estimated  $K_D$  which is ratio of concentration of MB on the hydrogel composites containing 1 g of modified pumice at equilibrium ( $q_e$ ) to the remaining concentration of the dye in solution at equilibrium ( $C_e$ ). We plotted the logarithm of  $K_D$  against the inverse of temperature. By measuring the slope of this plot line with and its intercepts with the axis, we obtained the values of Enthalpy,  $\Delta H = 15.715$  kJ mol<sup>-1</sup> and Entropy  $\Delta S^\circ = 85.9$  J K<sup>-1</sup> mol<sup>-1</sup>.

These two values were used to measure  $\Delta G$ ,  $\Delta H$  and  $\Delta S$  according to the following equations [44]:

$$\ln K_D = \Delta S^\circ / R - \Delta H^\circ / RT \quad (3)$$

$$\Delta G^\circ = \Delta H^\circ - T \Delta S^\circ \quad (4)$$

where  $K_D$  is ratio of concentration of MB on adsorbent at equilibrium ( $q_e$ ) to the remaining concentration of the dye in solution at equilibrium ( $C_e$ ).

To study the adsorption kinetics, the amount of adsorbed MB was evaluated using a UV spectrometer at  $\lambda_{\max} = 664$  nm and at time intervals of 10-150 min. At 25 °C for 24 hours, 0.05 g of the hydrogel composites were immersed in 50 mL of dye solutions containing 25, 50, 100, 150, and 200 mg L<sup>-1</sup> of MB.

### 1.5. Instrumental characterization

Fourier transform infrared (FTIR) spectroscopy was used to investigate the information on the structure of the kC-PVA-modified pumice composite hydrogels, scanning electron microscopy (SEM) was used to study surface morphology of the hydrogel composites, and X-Ray diffraction (XRD) was used to identify the atomic and molecular structure of the materials.

For the FTIR characterization, hydrogel composites samples were placed as KBr pellets in an FTIR spectrophotometer (Bruker, Germany) at room temperature. For identifying the morphology of hydrogels using SEM testing, the sample powder was dried for 48 hours at room temperature (25 °C). The dried sample powder was sputtered with a thin coating of palladium gold alloy and scanned in a SEM device equipped with an Energy Dispersive X-ray Analysis (EDX) Unit, model Quanta 250 Field Emission Gun (FEG) developed by FEI Company, Netherlands. The accelerating voltage of this device was 30 kV, and the magnification range is between 14-10000X.

The materials' X-ray diffraction patterns were recorded using a Siemens D-500 X-ray diffractometer at a wavelength of  $k = 1.54$  Å (Cu-K), a tube voltage of 35 kV, and a tube current of 30 mA.

## 3. Results and discussion

### 3.1. Characterization Results

#### 3.1.1 FTIR analysis

The results of the FTIR spectra are shown in Figure 3 for (1) the pumice-free hydrogel, (2) the hydrogel composite containing 0.2 g pumice, (3) the hydrogel composite containing 0.4 g pumice, (4) the hydrogel composite containing 0.6 g pumice, (5) the hydrogel composite containing 1 g pumice, the kC, the PVA and the modified pumice of this study. This figure indicates that for each material there are several bands; some of them are narrow while others are broad. The narrow bands detected in the kC spectra at 846, 922, 1043, and 1377 cm<sup>-1</sup> can be ascribed to D-galactose-4-sulfate, 3,6-anhydro-D-galactose, glycosidic linkage, and ester sulfate stretching, respectively. The wide band at 3200-3400 cm<sup>-1</sup> is caused by stretching of the substrate's -OH groups.

The FTIR spectrum of the pure PVA shows the C-O stretching band at 1095 cm<sup>-1</sup>, the C-C band at 1509 cm<sup>-1</sup>, the -CH band at 2939 cm<sup>-1</sup> and the broad band centered at approximately 3600 cm<sup>-1</sup> due to -OH stretching.

The characteristic bands in the modified pumice at roughly 525 and 1052 cm<sup>-1</sup> are attributed to the pumice's Si-O bands. The broad peak at around 3450 cm<sup>-1</sup> is attributed the stretching vibration of H<sub>2</sub>O molecules (moisture) in the lattice and also to -OH groups. The stretching vibration of -OH groups of water received from the external environment is

connected with the deformation peak at about 1640  $\text{cm}^{-1}$ .

The characteristic stretching vibrations of -Si-O and -Al-O groups were examined at 1043  $\text{cm}^{-1}$ , whereas the bending modes of groups were detected between 400 and 500  $\text{cm}^{-1}$ . The undistorted Si-O-Al framework is shown by the Si-O-Al stretching vibration, which was measured at 785  $\text{cm}^{-1}$ .

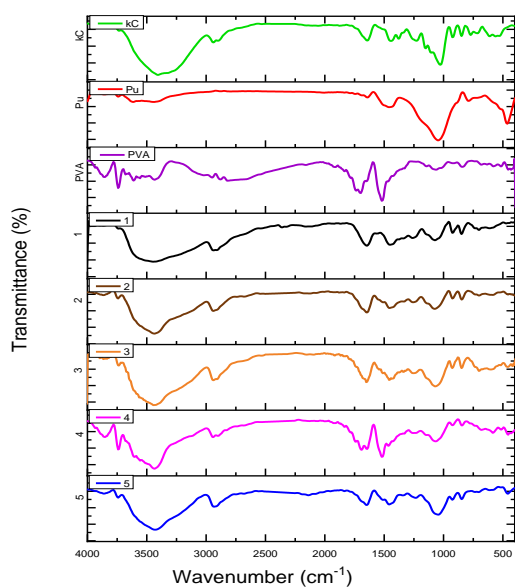


Figure 3. FTIR spectra of the materials of this study: kC, PVA, modified pumice, (1) Pure hydrogel composites without pumice, (2) Hydrogel composite containing 0.2 g of pumice, (3) Hydrogel composite containing 0.4 g of pumice, (4) Hydrogel composite containing 0.6 g of pumice, (5) Hydrogel composite containing 1 g of pumice.

Speaking of the spectrum of pumice-free composite hydrogels, it was shown that the absorption band which appeared at 3300–3600  $\text{cm}^{-1}$  is attributed to -OH stretching vibrations due to intermolecular and intra-molecular hydrogen bonds. Due to the existence of diverse OH groups in both PVA and kC, this band may become broader with the addition of kC content in contrast to the pure PVA sample. Meanwhile, as a result of the intermolecular hydrogen bond interactions between PVA and kC, the distinctive band of 3441  $\text{cm}^{-1}$  for pure PVA has migrated to lower wavenumbers. It is thought that the addition of kC to the PVA system can prevent both the collapse of pores and morphology shrinkage with the structure during lyophilization (freeze drying). Such an in-depth and detailed understanding of the molecular interaction based on hydrogen bonding between PVA and kC, and also the crystallization behavior of PVA when adding kC content was needed; therefore, the use of FT-IR spectrum helped in conducting such an investigation.

In regard to the hydrogel composite products containing pumice, it was found that, compared to pumice-free hydrogel; the intensity of the sulfate stretching band of kC in the hydrogel composite has diminished. This has aided in the creation of hydrogen bonds and crosslinks between these groups and Si-OH on the pumice surface layer. Further, it was found that the -CO stretching band of PVA and the -Si-O band of modified pumice were *slightly* overlapped and they became a broader band at approximately 1048  $\text{cm}^{-1}$ . It was also found that the -OH stretching bands of pumice (at approximately 3650  $\text{cm}^{-1}$ ) were shifted to a lower wave number towards the -OH stretching bands of PVA (at approximately 3200–3450  $\text{cm}^{-1}$ ) and they combined together to become a broader hydroxyl stretching band.

In summary, FT-IR spectroscopy of the materials revealed that incorporating modifying pumice into kC and PVA chains resulted in interactions between silanol and functional groups on polymers.

### 3.1.2. SEM analysis

Figure 4 shows the SEM images of surface of (1) the pumice-free hydrogel, (2) the hydrogel composite containing 0.2 g pumice, (3) the hydrogel composite containing 0.4 g pumice, (4) the hydrogel composite containing 0.6 g pumice, (5) the Hydrogel composite containing 1 g pumice, the kC, the PVA and the modified pumice of this study.

These images show that the pure PVA sample had a relatively smooth surface with a porosity pattern and pore diameters between 0.30 to 0.90  $\mu\text{m}$ , while the modified pumice sample had an even rougher surface than the PVA sample. In contrast, the kC sample had a smooth surface with no porosity. Although the surface of the pumice-free hydrogel was rather smooth, the SEM micrographs of the PVA-kC -modified pumice hydrogels clearly show their porous features. These pores are thought to be the areas where water permeates and the places where external stimuli interact with the hydrophilic groups (-OSO<sup>3-</sup>) of KC.

Due to pumice particles projecting onto the surface of hydrogel composites containing pumice, the surface roughness has grown; the roughness has increased in accordance with the rising ratio of pumice. Images 2 through 5 show that the pumice particles are evenly distributed throughout the hydrogel composite matrix in every example. These photos demonstrated that the porous samples had showed a uniform porosity structure.

Fig. 5 showed the energy-dispersive X-ray (EDX) chart for modified pumice, these certain that the modified pumice is natural pumice coated with manganese dioxide.

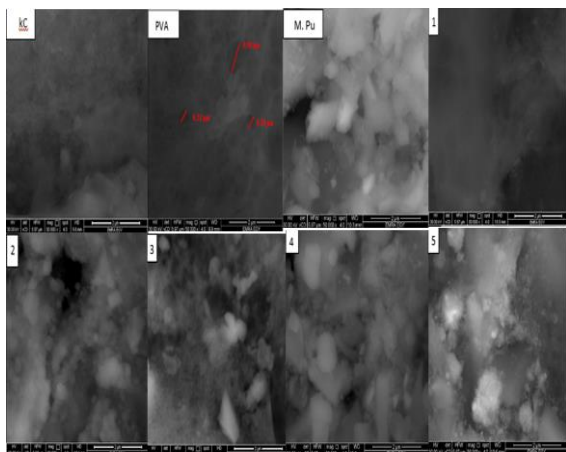


Figure 4. SEM images of PVA, kC modified pumice, (1) pure hydrogel composite without pumice, (2) Hydrogel composite containing 0.2 g of pumice, (3) Hydrogel composite containing 0.4 g of pumice, (4) Hydrogel composite containing 0.6 g of pumice and (5) Hydrogel composite containing 1 g of pumice.

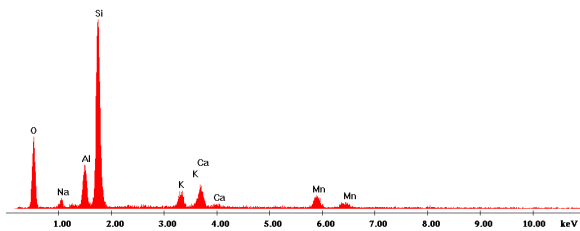


Figure 5: energy-dispersive X-ray scan of modified pumice.

### 3.1.3. XRD analysis

The results of XRD analysis are shown in Figure 6 for (1) the hydrogel composite without pumice, (5) the composites hydrogel with modified pumice 1 g, kC, PVA and modified pumice (M. Pu). These charts show that the carrageenan has a strong characteristic peak at  $2\theta = 8.5^\circ$  with a basal spacing of  $18 \text{ \AA}$ . However, this peak is not available for hydrogel composites without modified pumice (1) and with modified pumice 1g (5). This suggests a change in kC characteristics when forming the composite hydrogel.

The two beaks of pumice at  $29^\circ$  and  $52^\circ$  became smaller in magnitude in the hydrogel composite with 1g pumice which suggests a high dispersion of pumice in the composite material.

The sharp peaks of PVA at  $27^\circ$  and  $42^\circ$  where shifted to lower angles in the hydrogel composite without pumice (1) and they have further decreased more in the case of hydrogel composites containing 1g pumice (5). This may indicate changes to the characteristics of platelets of modified pumice while forming the composite hydrogels, they may have been exfoliated and became thoroughly dispersed in the polymer matrix after crosslinking and forming a composite structure.

In comparison with modified pumice, the peak of pumice has shifted, with a lower intensity, towards a lower angle  $2\theta = 29.0^\circ$  corresponding to a basal spacing of  $23 \text{ \AA}$ . This suggests that increasing the pumice content, in addition to exfoliation, may have resulted in the shift of XRD patterns of pumice and the hydrogel composites containing 1g pumice (5) and interlayer space due to polymer molecule intercalation.

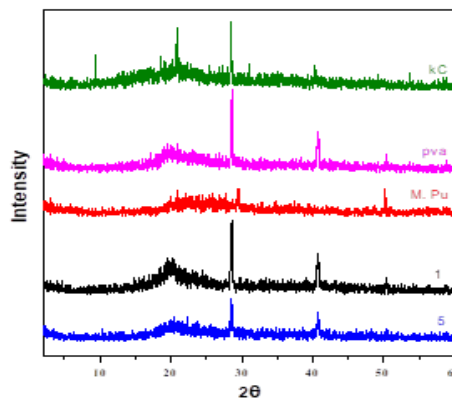


Figure 6: XRD patterns of kC, PVA, modified pumice, (1) pure hydrogel composite without pumice and (5) Hydrogel composite containing 1 g of pumice.

### 3.2. Swelling study

In general, the swelling capacity of hydrogels is strongly influenced by their chemical composition. To understand the effect of pumice on the swelling behavior of the hydrogels, the swelling capacity was investigated by varying the modified pumice content from 0.2 up to 1g (Fig. 7).

The results of the swelling capacity at equilibrium conduction (ES) are shown in Figure 7. This figure indicates that the ultimate swelling capacity at equilibrium has decreased as the modified pumice content has increased. This observation can be described by the interaction between the modified pumice layers and polymeric chains through formation of hydrogen bonding [45]. This interaction may lead to increases in the crosslinking points and therefore may it result in decreased swelling capacity [46]. These results are expected to happen although increasing the content of modified pumice may increase the surface area of the resulting composite hydrogels. However, the resultant products obtained without applying repeated freezing–thawing cycles were found not to possess good dimensional stability; therefore, the strength of swollen gel is not sufficient to be considered as a real cross-linked polymeric network.

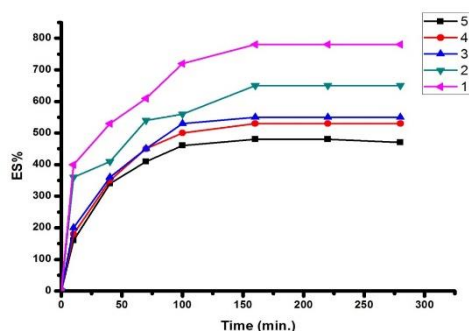


Figure 7. The swelling behavior of the pure hydrogel and the hydrogel composites with various content of modified pumice: (1) pumice-free composite hydrogel, (2) Hydrogel composite containing 0.2 g of pumice, (3) Hydrogel composite containing 0.4 g of pumice, (4) Hydrogel composite containing 0.6 g of pumice, (5) Hydrogel composite containing 1 g of pumice.

### 3.3. Dye adsorption study

#### 3.3.1. Effect of pH on dye adsorption

The pH of the initial dye solution is an important factor in adsorption process. This behaviour arises from the nature of the active centres on the adsorbents [47]. To investigate the adsorption of MB dye on adsorbents, the pH of the initial dye solution was changed between 2 and 10 and the results are shown in Fig. 8.

The results of effect of pH on the adsorption of MB dye are shown in Figure 8. This figure shows that the ratio of adsorbed MB dye to the initial content of this dye is generally high and reaching as high as 97.48 %. Additionally, as the content of pumice increases, this ratio of adsorbed MB dye also increases, though marginally. It also shows that as the degree of pH increases, from 2 to 8, the ratio of adsorbed MB dye also increases, though marginally. However, interestingly, strong alkali solutions where pH=10 and strong acidic solutions where pH=2 have resulted in exact adsorption ratios of MB. These results are understood as follows.

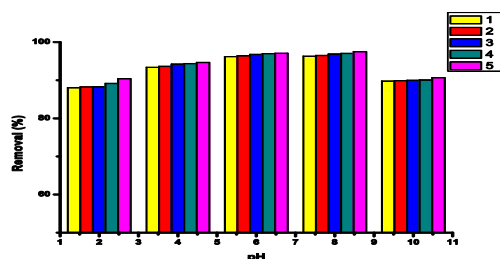


Figure 8. Effect of pH of initial dye solution on MB adsorption: (1) pumice-free composite hydrogel, (2) Hydrogel composite containing 0.2 g of pumice, (3) Hydrogel composite containing 0.4 g of pumice, (3) Hydrogel composite containing 0.6 g of pumice, (5) Hydrogel composite containing 1 g of pumice.

During adsorption, the existence of anionic sulfate groups is necessary for the interaction of hydrogel composite with positively charged MB molecules, as is simply shown in Figure 9. Compared to hydrogels carrying carboxylate pendants, the adsorption capacity of kC-based hydrogels for MB was only changed marginally in the pH range of 2–10. This behavior originated from the pKa of anionic sulfate groups on kC. According to literatures, the pKa of these anionic sulfates is around 2 and its ionization occurs above this value [48, 49]. At pH 2, a small reduction in dye affinity for hydrogels was seen and this may be attributed to the screening effect of the counter ions ( $H^+$ ) that restricts the approaching of cationic dye to sulfate groups. In fact, in the overall pH range, these sulfate groups are in the dissociated form. Lower adsorption of MB at the *strong* acidic solutions is explained by the presence of excess  $H^+$  ions competing with the cation groups on the dye for adsorption sites. The highest adsorption at pH 8 and pH 6, which are close to neutral pH, is explained as follows. At Low pH values, the high percentage of hydrogen cations within the solution creates an electrical cloud around the prepared hydrogel composite and this in turn leads to electric repulsion of the cationic MB dye. However, at higher pH levels, MB dye uptake decreases because some of the dye precipitate.

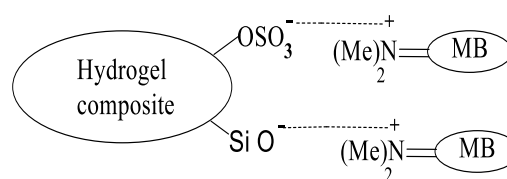


Figure 9. Electrostatic interactions between negative and positive functional groups of the hydrogel composite and cationic methylene blue (MB) dye molecules.

#### 3.3.2. Effect of pumice content and contact time on cationic methylene blue dye adsorption

The effect of both modified pumice content and contact time on the adsorption of MB on hydrogel composite is shown in Figure 10. This figure confirms the finding in Figure 9 and it also shows that the adsorption capacity of the hydrogel composites increased with time and content of modified pumice. The increase in MB adsorption with the content of pumice may be attributed to both the negative surface and large specific surface area of modified pumice. This means that the higher the content of modified pumice in the hydrogel composites with a constant weight ratio of kC and PVA, the higher the concentration of negative charges on the surface of the composite hydrogels. Since MB is cationic dye, this increases its attraction to the negative pumice charges in the composite hydrogels. In fact, modified pumice is already

reported as good adsorbents for various adsorbates due to these two reasons. Figure 10 also demonstrates that, given the experimental conditions of this study, the adsorption capacity of MB was increased by increasing agitation time up to 90 min. However, further increases in the agitation time had no effect on  $q_e$ . It is obvious that increasing adsorption time provides high opportunity for interaction between the adsorbent and the adsorbate, within limits. That is, equilibrium was attained after 90 min, within the concentration range studied.

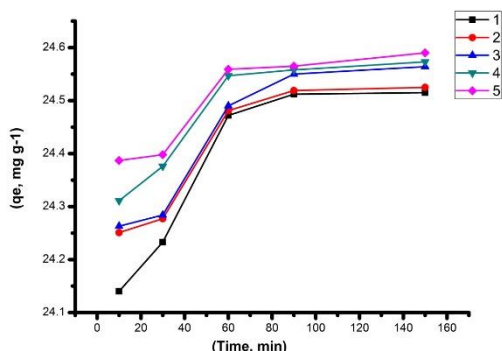


Figure 10. Effect of content of modified pumice and contact time on MB adsorption on composite hydrogels: (1) pumice-free composite hydrogel, (2) Hydrogel composite containing 0.2 g of pumice, (3): Hydrogel composite containing 0.4 g of pumice, (3) Hydrogel composite containing 0.6 g of pumice, (5) Hydrogel composite containing 1 g of pumice.

### 3.3.3. Effect of salt solution on dye adsorption

The effect of different salts on adsorption of MB on hydrogels is presented in Figure 11. This figure indicates that the the adsorption capacity of hydrogels has decreased when salts were introduced to the MB dye solution. The degree of reduction is related to both the type of salt and the amount of pumice within the composite hydrogels. As the content of pumice increases, the reduction percentage decreases.

Typically, most dyes have hydrophobic structure, and the solubility of these dyes is reduced in the presence of salt. This reduction in the solubility of dyes originated from increasing in polarity of the solution. The results of which is mainly an enhancement in dye adsorption is observed [50], however, in the case of adsorbents with ionic pendants, often a reduction in dye adsorption is obtained. Therefore, in our study, by introducing NaCl in dye solution, the adsorption capacity of hydrogels was slightly decreased.

The neutralisation or screening of anionic sulphate ( $-\text{OSO}_3^-$ ) groups on kC by metal ions is responsible for the corresponding reduction in the dye adsorption capability of hydrogel composites [50, 51]. The electrostatic interactions between anionic sulphate groups on the adsorbent and cationic dyes

may be lessened as a result of this effect. The adsorption capacity of hydrogels for MB dye in dye solutions containing  $\text{CaCl}_2$  and  $\text{AlCl}_3$  salts was substantially lower than in NaCl solution. The  $\text{Ca}^{2+}$  and  $\text{Al}^{3+}$  ions' interaction with the anionic centres of hydrogels is what causes this phenomenon. These compounds might cause hydrogels to swell less and hence have less surface area. Such a decrease in hydrogels' surface could therefore result in dye adsorption capacity.

This reduction in the solubility of dyes is originated from increasing in polarity of the solution. In contrast, in the adsorbents with ionic pendants, often a reduction in dye adsorption is obtained.

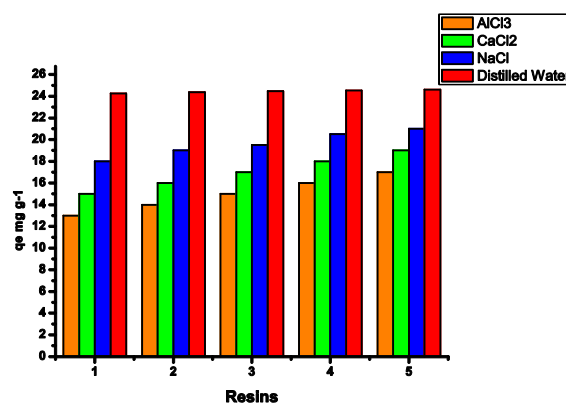


Figure 11: Effect of salts with the MB dye solution on their adsorption on composite hydrogels: (1) pumice-free composite hydrogel, (2) Hydrogel composite containing 0.2 g of pumice, (3): Hydrogel composite containing 0.4 g of pumice, (4) Hydrogel composite containing 0.6 g of pumice, (5) Hydrogel composite containing 1 g of pumice.

### 3.3.4. Effect of temperature on dye adsorption: Relevant thermodynamic parameters

By plotting the logarithm of  $K_D$  against the inverse of temperature Figure 12 has resulted. This plot indicated a strong linear relationship as indicated by the value of Coefficient of Determination  $R^2 = 0.9741$ .

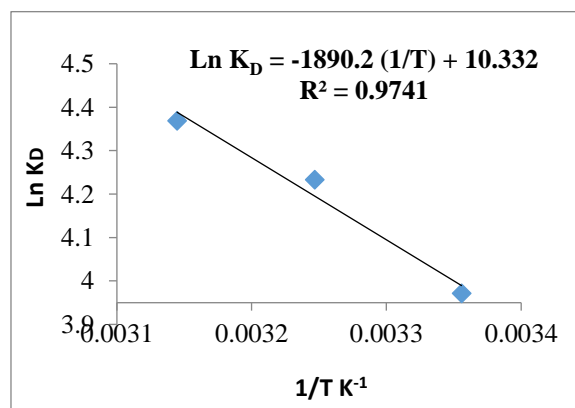


Figure 12. Plot of  $\text{Ln } K_D$  versus  $1/T$  for the hydrogel composites containing 1 g of modified pumice.

Table 1 displays the computed thermodynamic parameters for the adsorption of MB dye. The absence of  $\Delta G^\circ$  values at the examined temperatures shows that the MB dye adsorption on the hydrogel composites is spontaneous and possible from a thermodynamic perspective [52]. Additionally, the  $\Delta G^\circ$  values fell from 298 to 318 K, indicating a high driving force and, thus, a larger adsorption capacity at higher temperatures. Additionally, as the adsorption is endothermic in nature as indicated by the positive values of  $\Delta H^\circ$  [53], the process may be more advantageous at higher temperatures. However, the increased unpredictability of the adsorbed dye molecules on composite surfaces is indicated by the positive  $\Delta S^\circ$  value. [53].

Therefore, due to electrostatically interactions between anionic sulfate groups of kC and cationic MB molecules, the adsorption is spontaneous and endothermic due to differences in electrical charges and thus creating the conditions for electrical attraction.

Table 1 Thermodynamic parameters for the adsorption of MB onto hydrogel composites containing 1 g content of modified pumice:

T (K)	Thermodynamic parameters			R <sup>2</sup>
	$\Delta G^\circ$ (kJ mol <sup>-1</sup> )	$\Delta S^\circ$ (J K <sup>-1</sup> mol <sup>-1</sup> )	$\Delta H^\circ$ (kJ mol <sup>-1</sup> )	
298	-9.88	85.9	15.715	0.974
308	-10.74			
318	-11.6			

### 3.4. Adsorption kinetics

The kinetic parameters can be used to forecast the rate of adsorption, which is crucial information for adsorption effectiveness. Therefore, faux first order and pseudo second order kinetic models were employed to illustrate which model was most appropriate for the experimental kinetic data. The pseudo-first-order rate equation's linear version is given as [54]

$$\ln (q_e - q_t) = \ln q_{e1} - k_1 t$$

where  $q_e$  and  $q_t$  are the amounts of MB adsorbed (mg g<sup>-1</sup>) at equilibrium and at a predetermined time (t), respectively.  $q_{e1}$  and  $k_1$  (min<sup>-1</sup>) show the theoretical equilibrium adsorption and rate constant of pseudo-first-order kinetic, respectively. The linear form of the pseudo-second-order rate equation is expressed as[54]:

$$t/q_t = 1/k_2 q_e^2 + t/q_e \quad (6)$$

where  $k_2$  (g mg<sup>-1</sup> min<sup>-1</sup>) is the pseudo-second-order rate constant and  $q_e$  is the theoretical adsorbed dye (mg g<sup>-1</sup>). To obtain model calculations for pseudo-first-order and pseudo-second-order kinetics, we plotted  $\ln (q_e - q_t)$  against t and  $t/q_t$  against t (Fig. 13,14). The obtained kinetic parameters and correlation coefficients (R<sup>2</sup>) are summarized in Table 2.

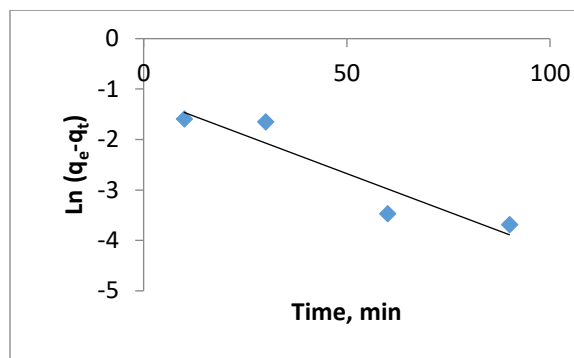


Fig. 13 Plots of  $\ln (q_e - q_t)$  vs. time in pseudo-first-order equation for the hydrogel composite containing 1 g content of modified pumice.

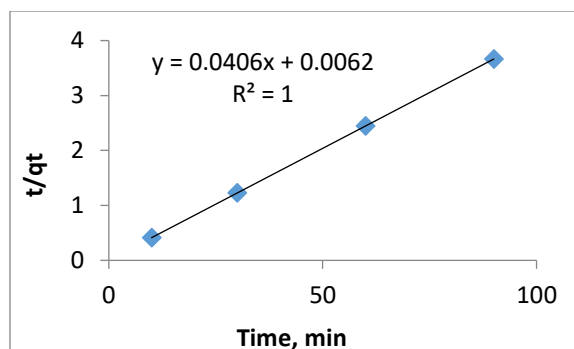


Fig. 14 Plots of  $t/q_t$  vs. time in pseudo-second-order equation for the hydrogel composite containing 1 g content of modified pumice.

The fits of experimental kinetic data to the above-mentioned rate models were evaluated by R<sup>2</sup>. The values of R<sup>2</sup> for the pseudo-second-order model were 1 for all samples, and the adsorption capacities calculated ( $q_{e2}$ ) by this model were also closer to those determined by experiments ( $q_{e,exp}$ ). These findings suggested that the pseudo-second-order rate model suited the adsorption process of MB on hydrogel composites better than the pseudo-first-order rate model. In actuality, the pseudo-second-order model is predicated on the premise that the rate-determining step might be chemical sorption involving valence forces via electron sharing or exchange between adsorbent and adsorbate.

### 1.5. Adsorption isotherms

The relationship between the amount of dye that has been adsorbed on the adsorbent and the dye concentration that is still present at equilibrium is expressed by the adsorption isotherm. In order to describe the adsorption process in this work, the experimental data from adsorption isotherms were fitted to non-linear Langmuir and Freundlich models[55, 56]. The monolayer adsorption of the adsorbate on certain homogenous sites inside the adsorbent is described by the Langmuir model. The expression of this non-linear model is in Eq. (7) [57]:

$$q_e = Q_o K_L C_e / (1 + K_L C_e) \quad (7)$$

Langmuir adsorption parameters were determined by transforming the Langmuir equation (8) into linear form.

$$1/q_e = 1/Q_o + 1/Q_o K_L C_e \quad (8)$$

where  $C_e$  is the equilibrium dye concentration in the solution ( $\text{mg L}^{-1}$ ),  $K_L$  is the Langmuir adsorption constant related to the energy of adsorption ( $\text{L mg}^{-1}$ ), and  $Q_o$  is the maximum adsorption capacity ( $\text{mg g}^{-1}$ ). Dimensionless constant adsorption parameter RL as one of the vital characteristics of the Langmuir isotherm is expressed as follows [58]:

$$RL = 1 / (1 + K_L C_o) \quad (9)$$

where  $K_L$  is the Langmuir constant ( $\text{L mg}^{-1}$ ) and  $C_o$  is the initial concentration of dye. In fact, the RL value describes the type and shape of the isotherm [58] as summarized in Table 3.

In distinction to the Langmuir model, the Freundlich model uses multilayer sorption to adsorb the adsorbate on a heterogeneous surface. Here is how the non-linear Freundlich model is defined [57]:

$$Q_e = K_F C_e^{1/n} \quad (9)$$

Linearizing the above equation, we have:

$$\log Q_e = \log K_F + 1/n \log C_e \quad (10)$$

where  $K_F$  is the equilibrium adsorption coefficient ( $\text{mg g}^{-1}$ ) ( $\text{L mg}^{-1}$ ) $^{1/n}$  and  $1/n$  is the empirical constant. The  $n$  value depicts the favorability of adsorption process and  $K_F$  is related to the adsorption capacity of adsorbent.

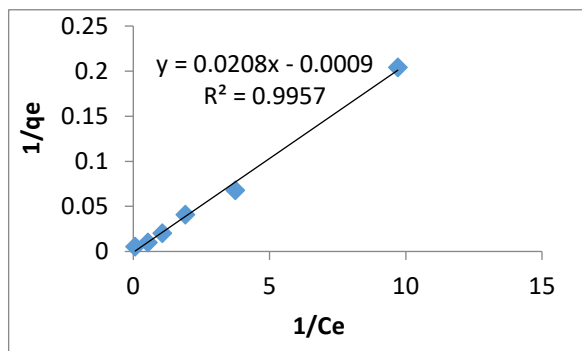


Fig (15). Langmuir Adsorption Isotherm

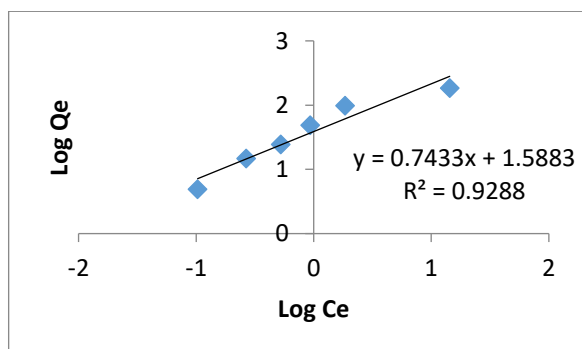


Fig (16). Freundlich Adsorption Isotherm

The extreme hydrogel adsorption capability determined by the Langmuir model was largely consistent with experimental results. This fitting demonstrated that dye is adsorbed on hydrogel adsorbents in a monolayer. The values of RL for hydrogels were also estimated using the Langmuir model, and they were discovered to be advantageous adsorption system values between 0 and 1. (see also Table 3). Finally, Table 6 compares the maximal adsorption capacity of the current study to other dye adsorbents described in the literature. These data show that the hydrogel composites created for this investigation had an adsorption capacity that was comparable to that of other adsorbents.

### Temkin Isotherm

This isotherm has a component that obviously accounts for the interactions between the adsorbent and adsorbate. The model makes the assumption that the heat of adsorption (a function of temperature) of all molecules in the layer will drop linearly rather than logarithmically with coverage by disregarding the extremely low and high concentration values [[59],[60]]. By graphing the amount sorbed  $q_e$  against  $\ln C_e$ , it was possible to demonstrate that, as predicted by the equation, its derivation is characterized by a uniform distribution of binding energies (up to some maximum binding energy). The constants were then derived from the slope and intercept. Using the following equation, the model is provided.[59]:

$$q_e = RT/b \ln (A_T C_e) \quad (12)$$

$$q_e = RT/b_T \ln A_T + (RT/b \ln C_e) \quad (13)$$

$$B = RT/b_T \quad (14)$$

$$q_e = B \ln A_T + B \ln C_e \quad (15)$$

$A_T$  = Temkin isotherm equilibrium binding constant ( $\text{L/g}$ )

$b_T$  = Temkin isotherm constant

$R$  = universal gas constant  $8.314 \text{ (J/mol/K)}$

$T$  = Temperature at  $298\text{K}$ .

$B$  = Constant related to heat of sorption( $\text{J/mol}$ )

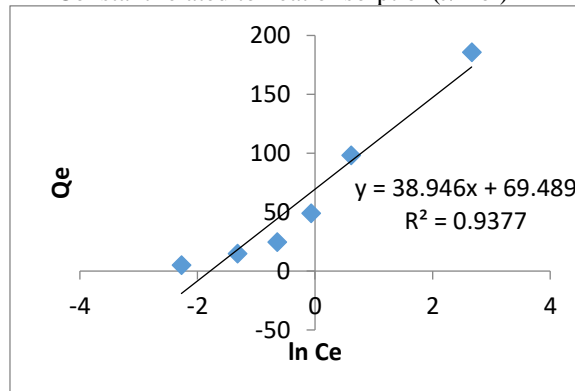


Fig (17). Temkin Adsorption Isotherm

Table 2 Constants of pseudo-first order and pseudo-second-order rate models for MB adsorption onto hydrogel composites

Samples	First-order kinetics			Second-order kinetics			q <sub>e,exp</sub>
	k <sub>1</sub> × 10 <sup>-3</sup>	R <sup>2</sup>	q <sub>e1</sub>	k <sub>2</sub> × 10 <sup>-3</sup>	R <sup>2</sup>	q <sub>e2</sub>	
pumice 0g (1)	61.8	0.9474	1.147	141.58	1	24.57	24.51
Pumice 0.2g (2)	49.9	0.9756	0.6977	174.37	1	24.57	24.525
Pumice 0.4g (3)	39.9	0.9401	0.6435	158.5	1	24.63	24.564
Pumice 0.6g (4)	39.6	0.9347	0.4389	219.79	1	24.63	24.573
Pumice 1g (5)	30.3	0.8764	0.3132	274.74	1	24.63	24.59

Table 3: RL values and isotherms

RL value	Type of isotherm
RL > 1	Unfavorable
RL = 1	Linear
0 < RL < 1	Favorable
RL = 0	Irreversible

From the Temkin plot shown in fig 13, the following values were estimated: A<sub>T</sub> = 5.95 L/g, B=38.946 (J/mol) which is an indication of the heat of sorption indicating a physical adsorption process and the R<sup>2</sup>=0.94.

Table 4: Parameters for plotting Langmuir, Freundlich, Temkin and Dubinin-Radushkevich Adsorption Isotherms for MB adsorption onto hydrogel composites

S/N	C <sub>0</sub> (mg/L)	C <sub>e</sub> (mg/L)	1/C <sub>e</sub>	Log C <sub>e</sub>	Ln C <sub>e</sub>	Q <sub>e</sub> (mg/g)	1/Q <sub>e</sub>	Log Q <sub>e</sub>	Ln Q <sub>e</sub>	C <sub>0</sub> /Q <sub>e</sub> g/L	ε <sup>2</sup>
1	0	0	0	0	0	0	0	0	0	0	0
2	5	0.103	9.709	-0.987	-2.273	4.897	0.204	0.689	1.589	0.021	3.45×10 <sup>7</sup>
3	15	0.267	3.745	-0.573	-1.321	14.733	0.068	1.168	2.690	0.018	1.49×10 <sup>7</sup>
4	25	0.525	1.905	-0.279	-0.644	24.475	0.041	1.389	3.198	0.021	6.98×10 <sup>6</sup>
5	50	0.935	1.069	-0.029	-0.067	49.065	0.020	1.691	3.893	0.019	3.25×10 <sup>6</sup>
6	100	1.85	0.540	0.267	0.615	98.15	0.010	1.992	4.586	0.019	1.15×10 <sup>6</sup>
7	200	14.35	0.069	1.157	2.664	185.65	0.005	2.269	5.224	0.077	2.79×10 <sup>4</sup>

Table 5: Langmuir, Freundlich, Temkin and Dubinin–Radushkevich Isotherm constants for the adsorption for MB adsorption onto hydrogel composites.

LANGMUIR ISOTHERM				FREUNDLICH ISOTHERM			
Q <sub>0</sub> (mg/g)	KL (L/m g)	RL	R <sup>2</sup>	1/n	n	K <sub>f</sub> (mg/g)	R <sup>2</sup>
1111.1	0.0433	0.3287	0.9957	0.7433	1.345	38.753	0.9288
TEMKIN ISOTHERM				DUBININ – RADUSHKEVICH ISOTHERM			
A <sub>T</sub> (L/g)	b <sub>T</sub>	B	R <sup>2</sup>	q <sub>s</sub> (mg/g)	K <sub>ad</sub> (mol <sup>2</sup> /KJ <sup>2</sup> )	E (KJ/mol)	R <sup>2</sup>
5.95	63.616	38.946	0.9377	87.226	9×10 <sup>-8</sup>	0.16667	0.8449

Table 6 Comparison of sorption capacity of (MB) on various adsorbents.

Adsorbent name	Adsorbent dosage (g/L)	Initial dyes concentration (mg/L)	Maximum adsorption capacity (mg/g)	References
Poly(vinyl alcohol)/carboxymethyl cellulose/graphene oxide/bentonite	1.5	200	172.14	[61]
Poly(vinyl alcohol)/carboxymethyl cellulose/ZSM-5 zeolite	1.25	10	7.8	[62]
Modified polysaccharide	0.5	50	48	[63]
Hydrolyzed Oak sawdust	2.5	300	67.78	[64]
Activated carbon	5	25	8.77	[65]
cotton stalk	4	825	111.36	[66]
Water Hyacinth Root Powder	1	10	8.04	[67]
Pea shells (Pisum sativum)	1	350	246.91	[68]
kC–PVA/M. pumice	1	200	185.65	Present work

Where B<sub>DR</sub> is denoted as the isotherm constant. Meanwhile, the parameter ε can be calculated as:

### Dubinin–Radushkevich isotherm model

On a heterogeneous surface, the Dubinin–Radushkevich isotherm is usually used to describe the adsorption mechanism with a Gaussian energy distribution [69, 70]. The results from the intermediate range of concentrations and high solute activity have frequently been well fit by the model.

$$q_e = (q_s) \exp(-K_{ad} \epsilon^2) \quad (16)$$

$$\ln q_e = \ln(q_s) - (K_{ad} \epsilon^2) \quad (17)$$

Where  $q_e$  = amount of adsorbate in the adsorbent at equilibrium (mg/g);  $q_s$  = theoretical isotherm saturation capacity (mg/g); and  $\epsilon$  = Dubinin–Radushkevich isotherm constant ( $\text{mol}^2/\text{kJ}^2$ ). The method was frequently used to differentiate between the physical and chemical adsorption of metal ions with its mean free energy,  $E$  per molecule of adsorbate (for removing a molecule from its location in the sorption space to infinity), which may be calculated by the connection [71, 72].

$$E = [1/\sqrt{2K_{ad}}] \quad (18)$$

$$\epsilon = RT \ln [1 + 1/C_e] \quad (19)$$

where  $R$ ,  $T$  and  $C_e$  represent the gas constant (8.314 J/mol K), absolute temperature (K) and adsorbate equilibrium concentration (mg/L), respectively. One of the unique features of the Dubinin–Radushkevich (DRK) isotherm model lies on the fact that it is temperature-dependent, which when adsorption data at different temperatures are plotted as a function of logarithm of amount adsorbed ( $\ln q_e$ ) vs  $\epsilon^2$  the square of potential energy, all suitable data will lie on the same curve, named as the characteristic curve [73]. The equation (16) is linearized to equation 17 which is used in the plot of DRK graph in figure 14. The constants such as  $q_s$ , and  $K_{ad}$  were determined from the appropriate plot using equation 17 above. From the linear plot of DRK model,  $q_s$  was determined to 87.23 mg/g, the mean free energy,  $E=0.167\text{KJ/mol}$  indicating a physio sorption process and the  $R^2=0.84$  lower than that of Temkin.

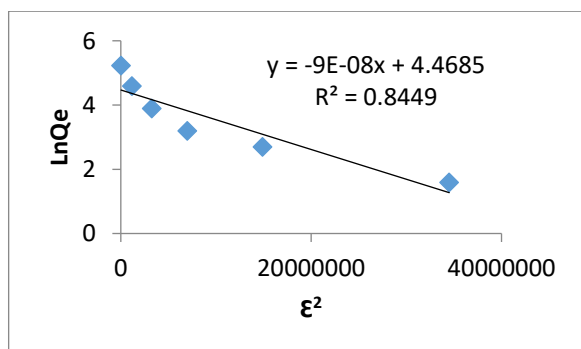


Fig (18). Dubinin–Radushkevich adsorption Isotherm

### Conclusion

In the current investigation, a new hydrogel composite of kappa carrageenan and poly(vinyl alcohol) was synthesised by freezing–thawing technique in the presence of modified pumice (Birm). Particular interactions of modified pumice (Birm)

with functional groups of kC and PVA through hydrogen bonding were estimated by FTIR. Also, XRD showed a layered morphology due to the penetration of polymer chains into modified pumice (Birm) silicate layers. According to XRD results, the modified pumice (Birm) showed intercalated and exfoliated structure. The modified hydrogel composite was then used for removal of methylene blue from aqueous solution. The adsorption capacity of composites was found to vary with content of modified pumice (Birm), pH, salt solution, and contact time as well as temperature of solution. Thermodynamic parameters also indicated that the adsorption was spontaneous and endothermic in nature.

Moreover, the fitting of experimental kinetic data to rate models showed that the pseudo-second-order model was the best fitted than the pseudo-first-order model in adsorption of MB onto composites. Besides, the data indicated that the MB adsorption onto the hydrogel composites obeys the Langmuir isotherm model. According to this model, maximum dye adsorption capacity was achieved 185.65 mg g<sup>-1</sup>. Overall, the obtained results suggested that the hydrogel composites synthesized in this work could be used as an effective adsorbent for adsorption of MB in the field of wastewater treatment.

### References

- [1]. I.J.I.J.O.B. MACROMOLECULES, Xanthan gum/titanium dioxide nanocomposite for photocatalytic degradation of methyl orange dye, 121 (2019) 1046-1053.
- [2]. A. Cruz-Rizo, S. Gutiérrez-Granados, R. Salazar, J.M.J.S. Peralta-Hernández, P. Technology, Application of electro-fenton/bdd process for treating tannery wastewaters with industrial dyes, 172 (2017) 296-302.
- [3]. R. Acharya, B. Naik, K.J.N.i.t.W.P.o.T. Parida, Adsorption of cr (vi) and textile dyes on to mesoporous silica, titanate nanotubes, and layered double hydroxides, (2018) 219-260.
- [4]. K. Yamjala, M.S. Nainar, N.R.J.F.c. Ramiseti, Methods for the analysis of azo dyes employed in food industry—a review, 192 (2016) 813-824.
- [5]. E. Bazrafshan, M.R. Alipour, A.H.J.D. Mahvi, W. Treatment, Textile wastewater treatment by application of combined chemical coagulation, electrocoagulation, and adsorption processes, 57(20) (2016) 9203-9215.
- [6]. A.M. Isloor, M.C. Nayak, B. Prabhu, N. Ismail, A. Ismail, A.M.J.R. Asiri, F. Polymers, Novel polyphenylsulfone (ppsu)/nano tin oxide (sno2) mixed matrix ultrafiltration hollow fiber membranes: Fabrication,

- characterization and toxic dyes removal from aqueous solutions, 139 (2019) 170-180.
- [7]. A.M. Ashmawy, A.M. El-Sawy, A.A. Ali, S.M. El-Bahy, A.A.S. Alahl, Oxidative stability performance of new azophenol derivatives as antioxidants in working fluids for high-temperature solar applications, *Solar Energy Materials and Solar Cells* 230 (2021) 111282.
- [8]. A.A. Ali, M.M. Elsayy, S.S. Salem, A.A. El-Henawy, H. Abd El-Wahab, Preparation and evaluation of antimicrobial thiadiazol azo disperse dyes as colored materials in digital transfer printing ink for printing onto polyester fabric, *Pigment & Resin Technology* (2021).
- [9]. F. Mashkoo, A.J.J.o.M. Nasar, M. Materials, Magsorbents: Potential candidates in wastewater treatment technology—a review on the removal of methylene blue dye, 500 (2020) 166408.
- [10]. M. Yagub, T. Sen, S. Afroze, H. Ang, Dye and its removal from aqueous solution by adsorption: A review. *Adv colloid interfac* 209: 172–184, 2014.
- [11]. M. Vakili, M. Rafatullah, B. Salamatinia, A.Z. Abdullah, M.H. Ibrahim, K.B. Tan, Z. Gholami, P.J.C.p. Amouzgar, Application of chitosan and its derivatives as adsorbents for dye removal from water and wastewater: A review, 113 (2014) 115-130.
- [12]. J. Fang, B. Gao, A. Mosa, L.J.C.S. Zhan, Bioavailability, Chemical activation of hickory and peanut hull hydrochars for removal of lead and methylene blue from aqueous solutions, 29(1) (2017) 197-204.
- [13]. M. Rafatullah, O. Sulaiman, R. Hashim, A.J.J.o.h.m. Ahmad, Adsorption of methylene blue on low-cost adsorbents: A review, 177(1-3) (2010) 70-80.
- [14]. Z.-Y.J.J.o.C.U.o.M. Yang, Technology, Kinetics and mechanism of the adsorption of methylene blue onto acfs, 18(3) (2008) 437-440.
- [15]. M. Raffatulah, O. Sulaiman, R. Hashim, A.J.J.C.E. Ahmad, Adsorption of methylene blue on low-cost adsorbent: A review, 177 (2010) 7080.
- [16]. A.M. Elgarahy, H.Y. Mostafa, E.G. Zaki, S.M. ElSaeed, K.Z. Elwakeel, A. Akhdhar, E. Guibal, Methylene blue removal from aqueous solutions using a biochar/gellan gum hydrogel composite: Effect of agitation mode on sorption kinetics, *International Journal of Biological Macromolecules* (2023) 123355.
- [17]. E. Santoso, R. Ediati, Y. Kusumawati, H. Bahruji, D. Sulistiono, D.J.M.T.C. Prasetyoko, Review on recent advances of carbon based adsorbent for methylene blue removal from waste water, 16 (2020) 100233.
- [18]. Y. Yang, Q. Zhu, X. Peng, J. Sun, C. Li, X. Zhang, H. Zhang, J. Chen, X. Zhou, H. Zeng, Hydrogels for the removal of the methylene blue dye from wastewater: A review, *Environmental Chemistry Letters* (2022) 1-21.
- [19]. N. Dafader, M. Manir, M. Alam, S.P. Swapna, T. Akter, D. Huq, Effect of kappa-carrageenan on the properties of poly (vinyl alcohol) hydrogel prepared by the application of gamma radiation, *SOP Trans. Appl. Chem* 2 (2015) 1-12.
- [20]. H. Dai, Y. Huang, H. Huang, Eco-friendly polyvinyl alcohol/carboxymethyl cellulose hydrogels reinforced with graphene oxide and bentonite for enhanced adsorption of methylene blue, *Carbohydrate polymers* 185 (2018) 1-11.
- [21]. R. Sabarish, G. Unnikrishnan, Polyvinyl alcohol/carboxymethyl cellulose/zsm-5 zeolite biocomposite membranes for dye adsorption applications, *Carbohydrate polymers* 199 (2018) 129-140.
- [22]. M.I.H. Mondal, Cellulose-based superabsorbent hydrogels, Springer2019.
- [23]. C.M. Hassan, N.A. Peppas, Structure and applications of poly (vinyl alcohol) hydrogels produced by conventional crosslinking or by freezing/thawing methods, *Biopolymers· pva hydrogels, anionic polymerisation nanocomposites*, Springer2000, pp. 37-65.
- [24]. J.L. Holloway, A.M. Lowman, G.R.J.S.M. Palmese, The role of crystallization and phase separation in the formation of physically cross-linked pva hydrogels, 9(3) (2013) 826-833.
- [25]. R. Hernandez, D. Lopez, C. Mijangos, J.-M.J.P. Guenet, A reappraisal of the ‘thermoreversible’gelation of aqueous poly (vinyl alcohol) solutions through freezing–thawing cycles, 43(21) (2002) 5661-5663.
- [26]. J.S. Gonzalez, V.A.J.T.a. Alvarez, The effect of the annealing on the poly (vinyl alcohol) obtained by freezing–thawing, 521(1-2) (2011) 184-190.
- [27]. S.K. Mallapragada, N.A.J.J.o.P.S.P.B.P.P. Peppas, Dissolution mechanism of semicrystalline poly (vinyl alcohol) in water, 34(7) (1996) 1339-1346.
- [28]. S. Deng, H. Xu, X. Jiang, J. Yin, Poly (vinyl alcohol)(pva)-enhanced hybrid hydrogels of hyperbranched poly (ether amine)(hpea) for selective adsorption and separation of dyes, *Macromolecules* 46(6) (2013) 2399-2406.
- [29]. C.M. Hassan, N.A. Peppas, Structure and morphology of freeze/thawed pva hydrogels, *Macromolecules* 33(7) (2000) 2472-2479.

- [30]. J.O. Kim, J.K. Park, J.H. Kim, S.G. Jin, C.S. Yong, D.X. Li, J.Y. Choi, J.S. Woo, B.K. Yoo, W.S. Lyoo, Development of polyvinyl alcohol–sodium alginate gel-matrix-based wound dressing system containing nitrofurazone, *International journal of pharmaceutics* 359(1-2) (2008) 79-86.
- [31]. J. Pająk, M. Ziemski, B. Nowak, Poly (vinyl alcohol)–biodegradable vinyl material, *Chemik* 64 (2010) 523-530.
- [32]. X. Yang, K. Yang, S. Wu, X. Chen, F. Yu, J. Li, M. Ma, Z. Zhu, Cytotoxicity and wound healing properties of pva/ws-chitosan/glycerol hydrogels made by irradiation followed by freeze–thawing, *Radiation Physics and Chemistry* 79(5) (2010) 606-611.
- [33]. N.I. Torres, K.S. Noll, S. Xu, J. Li, Q. Huang, P.J. Sinko, M.B. Wachsman, M.L. Chikindas, Safety, formulation and in vitro antiviral activity of the antimicrobial peptide subtilisin against herpes simplex virus type 1, *Probiotics and antimicrobial proteins* 5(1) (2013) 26-35.
- [34]. A. Rasool, S. Ata, A. Islam, R.U.J.R.a. Khan, Fabrication of novel carrageenan based stimuli responsive injectable hydrogels for controlled release of cephadrine, 9(22) (2019) 12282-12290.
- [35]. E.R. Morris, D.A. Rees, G.J.J.o.m.b. Robinson, Cation-specific aggregation of carrageenan helices: Domain model of polymer gel structure, 138(2) (1980) 349-362.
- [36]. G. Pass, G. Phillips, D.J.M. Wedlock, Interaction of univalent and divalent cations with carrageenans in aqueous solution, 10(1) (1977) 197-201.
- [37]. K. Bongaerts, H. Reynaers, F. Zanetti, S.J.M. Paoletti, Equilibrium and nonequilibrium association processes of  $\kappa$ -carrageenan in aqueous salt solutions, 32(3) (1999) 683-689.
- [38]. D. Barloková, J.J.P.J.o.E.S. Ilavský, Removal of iron and manganese from water using filtration by natural materials, 19(6) (2010) 1117-1122.
- [39]. I. Anđelković, D. Manojlović, D. Đorđević, B. Dojčinović, G. Roglić, L.M.J.J.o.t.S.C.S. Ignjatović, Arsenic removal from aqueous solutions by sorption onto zirconium-and titanium-modified sorbents, 76(10) (2011) 1427-1436.
- [40]. N. Marsidi, H.A. Hasan, S.R.S. Abdullah, A review of biological aerated filters for iron and manganese ions removal in water treatment, *Journal of Water Process Engineering* 23 (2018) 1-12.
- [41]. J. Kalmár, G. Lente, I. Fábíán, Kinetics and mechanism of the adsorption of methylene blue from aqueous solution on the surface of a quartz cuvette by on-line uv–vis spectrophotometry, *Dyes and Pigments* 127 (2016) 170-178.
- [42]. L. Svoboda, N. Licciardello, R. Dvorský, J. Bednář, J. Henych, G. Cuniberti, Design and performance of novel self-cleaning g-c3n4/pmma/pur membranes, *Polymers* 12(4) (2020) 850.
- [43]. S. Deng, H. Xu, X. Jiang, J.J.M. Yin, Poly (vinyl alcohol)(pva)-enhanced hybrid hydrogels of hyperbranched poly (ether amine)(hpea) for selective adsorption and separation of dyes, 46(6) (2013) 2399-2406.
- [44]. A. Özcan, E.M. Öncü, A.S.J.J.o.H.m. Özcan, Adsorption of acid blue 193 from aqueous solutions onto dedma-sepiolite, 129(1-3) (2006) 244-252.
- [45]. Z. Darvishi, K. Kabiri, M. Zohuriaan-Mehr, A.J.J.o.A.p.s. Morsali, Nanocomposite super-swelling hydrogels with nanorod bentonite, 120(6) (2011) 3453-3459.
- [46]. G.B. Marandi, G.R. Mahdavinia, S.J.J.o.P.R. Ghafary, Collagen-g-poly (sodium acrylate-co-acrylamide)/sodium montmorillonite superabsorbent nanocomposites: Synthesis and swelling behavior, 18(6) (2011) 1487-1499.
- [47]. S. Chatterjee, T. Chatterjee, S.-R. Lim, S.H.J.B.t. Woo, Effect of the addition mode of carbon nanotubes for the production of chitosan hydrogel core–shell beads on adsorption of congo red from aqueous solution, 102(6) (2011) 4402-4409.
- [48]. J. Brady, J.J.C. Holum, Wiley: New. York, The study of matter and its changes, (1993) 769-813.
- [49]. Y.S. Gu, E.A. Decker, D.J.J.F.H. McClements, Influence of ph and carrageenan type on properties of  $\beta$ -lactoglobulin stabilized oil-in-water emulsions, 19(1) (2005) 83-91.
- [50]. Y. Hu, T. Guo, X. Ye, Q. Li, M. Guo, H. Liu, Z.J.C.E.J. Wu, Dye adsorption by resins: Effect of ionic strength on hydrophobic and electrostatic interactions, 228 (2013) 392-397.
- [51]. Q. Li, Q.-Y. Yue, H.-J. Sun, Y. Su, B.-Y.J.J.o.E.M. Gao, A comparative study on the properties, mechanisms and process designs for the adsorption of non-ionic or anionic dyes onto cationic-polymer/bentonite, 91(7) (2010) 1601-1611.
- [52]. A.N. Fernandes, C.A.P. Almeida, N.A. Debacher, M.M. de Souza Sierra, Isotherm and thermodynamic data of adsorption of methylene blue from aqueous solution onto peat, *Journal of Molecular Structure* 982(1-3) (2010) 62-65.
- [53]. S.M. Al-Mahmoud, Kinetic, isothermal and thermodynamic investigations for the use of pumpkin seed husks as low-cost biosorbent of solochrome cyanine r from aqueous solutions,

- Egyptian Journal of Chemistry 63(8) (2020) 2947-2957.
- [54]. S. Chatterjee, T. Chatterjee, S.-R. Lim, S.H. Woo, Effect of the addition mode of carbon nanotubes for the production of chitosan hydrogel core–shell beads on adsorption of congo red from aqueous solution, *Bioresource technology* 102(6) (2011) 4402-4409.
- [55]. H.R. Ali, H.Y. Mostafa, S. Husien, A. El-hoshoudy, Adsorption of btx from produced water by using ultrasound-assisted combined multi-template imprinted polymer (mips); factorial design, isothermal kinetics, and monte carlo simulation studies, *Journal of Molecular Liquids* 370 (2023) 121079.
- [56]. H. El-Sabban, M. Eid, Y. Moustafa, M. Abdel-Mottaleb, Pomegranate peel extract in situ assisted phytosynthesis of silver nanoparticles decorated reduced graphene oxide as superior sorbents for zn (ii) and lead (ii), *Egyptian Journal of Aquatic Biology and Fisheries* 24(1) (2020) 525-539.
- [57]. J. Piccin, C. Gomes, L. Feris, M.J.C.E.J. Gutterres, Kinetics and isotherms of leather dye adsorption by tannery solid waste, 183 (2012) 30-38.
- [58]. B. Hameed, A. Ahmad, N.J.C.E.J. Aziz, Isotherms, kinetics and thermodynamics of acid dye adsorption on activated palm ash, 133(1-3) (2007) 195-203.
- [59]. M. Tempkin, V. Pyzhev, Kinetics of ammonia synthesis on promoted iron catalyst, *Acta Phys. Chim. USSR* 12(1) (1940) 327.
- [60]. C. Aharoni, M. Ungarish, Kinetics of activated chemisorption. Part 2.—theoretical models, *Journal of the Chemical Society, Faraday Transactions 1: Physical Chemistry in Condensed Phases* 73 (1977) 456-464.
- [61]. H. Dai, Y. Huang, H.J.C.p. Huang, Eco-friendly polyvinyl alcohol/carboxymethyl cellulose hydrogels reinforced with graphene oxide and bentonite for enhanced adsorption of methylene blue, 185 (2018) 1-11.
- [62]. R. Sabarish, G.J.C.p. Unnikrishnan, Polyvinyl alcohol/carboxymethyl cellulose/zsm-5 zeolite biocomposite membranes for dye adsorption applications, 199 (2018) 129-140.
- [63]. A.T. Paulino, M.R. Guilherme, A.V. Reis, G.M. Campese, E.C. Muniz, J.J.J.o.C. Nozaki, I. Science, Removal of methylene blue dye from an aqueous media using superabsorbent hydrogel supported on modified polysaccharide, 301(1) (2006) 55-62.
- [64]. M. Abd El-Latif, A.M.J.D. Ibrahim, W. Treatment, Adsorption, kinetic and equilibrium studies on removal of basic dye from aqueous solutions using hydrolyzed oak sawdust, 6(1-3) (2009) 252-268.
- [65]. C.O. Ijagbemi, J.I. Chun, D.H. Han, H.Y. Cho, S.J. O, D.S.J.J.o.E.S. Kim, H.P. A, Methylene blue adsorption from aqueous solution by activated carbon: Effect of acidic and alkaline solution treatments, 45(8) (2010) 958-967.
- [66]. H. Deng, J. Lu, G. Li, G. Zhang, X.J.C.E.J. Wang, Adsorption of methylene blue on adsorbent materials produced from cotton stalk, 172(1) (2011) 326-334.
- [67]. M. Soni, A.K. Sharma, J.K. Srivastava, J.J.I.J.o.C.S. Yadav, Applications, Adsorptive removal of methylene blue dye from an aqueous solution using water hyacinth root powder as a low cost adsorbent, 3(3) (2012) 338-345.
- [68]. Ü. Geçgel, G. Özcan, G.Ç.J.J.o.C. Gürpınar, Removal of methylene blue from aqueous solution by activated carbon prepared from pea shells (*pisum sativum*), 2013 (2013).
- [69]. A. Günay, E. Arslankaya, I. Tosun, Lead removal from aqueous solution by natural and pretreated clinoptilolite: Adsorption equilibrium and kinetics, *Journal of hazardous materials* 146(1-2) (2007) 362-371.
- [70]. A. Dąbrowski, Adsorption—from theory to practice, *Advances in colloid and interface science* 93(1-3) (2001) 135-224.
- [71]. M. Dubinin, The potential theory of adsorption of gases and vapors for adsorbents with energetically nonuniform surfaces, *Chemical reviews* 60(2) (1960) 235-241.
- [72]. J.P. Hobson, Physical adsorption isotherms extending from ultrahigh vacuum to vapor pressure, *The Journal of physical chemistry* 73(8) (1969) 2720-2727.
- [73]. K.Y. Foo, B.H.J.C.e.j. Hameed, Insights into the modeling of adsorption isotherm systems, 156(1) (2010) 2-10.